Nonlinear Analysis: Modelling and Control, Vol. 28, No. 3, 431–446
https://doi.org/10.15388/namc.2023.28.31609

Vilnius University Press

Cattaneo–Christov heat flux impacts on MHD radiative natural convection of Al_2O_3-Cu-H_2O hybrid nanofluid in wavy porous containers using LTNE

Sameh E. Ahmed[a,b], **A. Mahdy**[b,1], **Mohamed A. Mansour**[c]

[a]Faculty of Science, King Khalid University,
Abha 62529, Saudi Arabia

[b]Faculty of Science, South Valley University,
Qena 83523, Egypt
mahdy@svu.edu.eg

[c]Faculty of Science, Assiut University,
Assiut, Egypt

Received: June 22, 2022 / **Revised:** January 19, 2023 / **Published online:** February 23, 2023

Abstract. This paper aims to examine impacts of Cattaneo–Christov heat flux on the magneto-hydrodynamic convective transport within irregular containers in the presence of the thermal radiation. Both of the magnetic field and flow domain are slant with the inclination angles Ω and γ, respectively. The worked fluid is consisting of water (H_2O) and Al_2O_3-Cu hybrid nanoparticles. The enclosures are filled with a porous medium, and the local thermal nonequilibrium (LTNE) model between the hybrid nanofluids and the porous elements are considered. Influences of various types of the obstacles are examined, namely, horizontal cold elliptic, vertical elliptic and cross section ellipsis. The solution methodology is depending on the finite volume method with nonorthogonal grids. The major outcomes revealed that the location $(0.75, 0.5)$ is better for the rate of the flow and temperature gradients. The higher values of H^* causes that the solid phase temperature has a similar behavior of the fluid phase temperature indicating to the thermal equilibrium state. Also, the fluid-phase average Nusselt number is maximizing by increasing Cattaneo–Christov heat flux factor.

Keywords: Cattaneo–Christov heat flux, wavy containers, hybrid nanofluids, LTNE technique, natural convection, nonorthogonal grid, radiation.

1 Introduction

Nanofluid composed of nanometer-sized solid elements such as fibers and tubes loaded in a liquid medium with the length scales of 1 to 100 nm. Commonly, metals, oxides and carbon nanotubes are implemented as nanoparticles in nanofluids. The worked regular

[1]Corresponding author.

fluids utilized frequently are water, methanol and ethylene glycol water. Nanoliquids have massive thermophysical features thermal conductivity, such as viscosity specific heat and stability, which possess an indispensable significant in heat transmission. Recently, the advanced class of nanoliquids, known as hybrid nanofluids, has shown encouraging enhancements in heat transmission attitude and thermophysical attributes in comparison to conventional nanoliquid. Some of scientists have exhibited the problems concerned with nanofluid of hybrid nanofluid from both theoretically or experimentally points of view. Mahdy et al. [11] reported a numerical simulation of buoyancy-driven flow of free convection heat transmission and entropy generation through a square porous container filled with hybrid nanofluids. The viscosity and thermal conductivity of the Al_2O_3-Cu/water hybrid nanofluid with volume fractions from 0.1% to 2% has been measured by Suresh et al. [27]. The outcomes revealed that both factors of the hybrid nanofluid boost with the solid volume nanosize particles concentrations. Nadeem et al. [16] discussed the flow of a non-Newtonian nanofluid stimulated by an oscillatory porous plate related to slip impact. A practically presented contribution concerned with cooling of solid elements of nanomaterials through a moving bed was analyzed by Turkyilmazoglu [28]. The analytical valuation of non-Newtonian of third grade nanofluid along an accelerated plate was presented by Khan and Shehzad [9]. Sundar et al. [26] synthesized a MWCNT-Fe_3O_4-H_2O hybrid nanomaterial, whilst a Titanum and Copper hybrid nanomaterial has been formed by Madhesh et al. [10]. Muhammad et al. [7] illustrated the fractional pattern of Brinkman sort fluid (BTF) holding hybrid nanosize particles. TiO_2-Ag nanoparticles were liquefied in H_2O as regular fluid to get a hybrid nanofluid. Numerical analysis has been introduced by Ahmed [1] for the convective transmission due to triangular fins within a slant trapezoidal non-Darcy porous container containing nanomaterial. Mansour et al. [13] argued the consequence of partial slip on mixed-radiative interaction convection flow of a micropolar hybrid nanomaterial with a slant magnetic field in an odd-shaped porous container with separated heating. Selimefendigil and Oztop [21] investigated numerically natural convection through a cavity due to a corrugated partition, which have varient liquids with different sections of the partition using carbon nanotube (CNT)-water nanofluid.

Thermal convection, conduction radiation represent the major kinds of heat transmission. Heat energy transport possesses an essential role in our daily life applications, i.e., heat absorption phenomenon, electronics, solar collectors, thermal and cooling system and engineering applications. With the intent of boosting the performance of variant energy systems, scientists have examined the energy transmission features of several nanofluids. Zheng et al. [31] illustrated the consequence of radiation-natural convection with entropy analysis of Al_2O_3-H_2O nanomaterials inside a slant container. Their outcomes illustrated that the maximum average Nusselt number and a total entropy are achieved at an anglethe of inclination $\pi/6$. Mansour et al. [14] reported a slant MHD mixed radiative-convection nanoliquid flow of a non-Newtonian hybrid through a slant lid-driven odd-shaped enclosure. House et al. [6] argued the case of natural convective heat transfer within a square container with heat-conducting obstacle placed at center, and they elucidated that the heat transmission weaken with a rising values of the solid obstacle length. Usman et al. [30] have argued that the radiation heat and mass transmission of

MHD flow enclosed in a square enclosure within two heated and two clod body. Usman et al. [29] addressed the significant consequences of nonlinear thermal radiation and unsteady thermal conductivity of rotating flow of hybrid nanofluid along a 3-dimension stretchable surface.

Since the prediction of heat transmission for curved surfaces (wavy or complex geometries) represents a topic of massive significance, it is watched in several engineering operations. It is necessary to analyze the heat transmission for more complex geometric shapes (e.g., containers with wavy and/or irregular sides). Engineering applications such as cooling systems of microelectronic apparatuses and wall bricks, heat exchangers, condensers in refrigerators, underground cable systems and heat transmission appeared in chemical reactors. Pop et al. [20] imposed the finite difference approach for analyzing the free convection in a partially heated wavy enclosure loaded by nanofluid. A numerical treatment of the mixed convection flow of Cu-H_2O nanofluid in a lid-driven cavity for variant aspect ratios employing the control volume technique has been provided by Muthtamilselvan et al. [15]. Abundant published papers concerned with simple and irregular cavities [3, 5, 8, 17, 18, 23].

Magnetohydrodynamics (MHD) points out an indispensable spectrum field of research that analyze the magnetic features of electrically conducting liquids. The flow and heat transmission phenomenon for a viscous liquid in the existence of magnetic field have massive applications in solar physics, chemical engineering, stellar, geophysics, optimization of solidification processes of metals and design of MHD power generators. Also, MHD flow has an indispensable role in the zone of medical science like magnetic resonance imaging, in the treatment of cancer tumour and other diagnostic tests. Sheikholeslami and Sadoughi [22, 24] discussed the lattice Boltzmann technique for MHD free convection nanofluid through a porous container for different shapes of nanoparticles and with elliptic inner cylinder. A numerical simulation of MHD free convection has been presented for a 2-dimensional triangular container with heated from below partially and cold oblique wall filled with nanoliquid by Mahmoudi et al. [12]. Biswas et al. [4] exhibited the thermal efficacy of half-sinusoidal variable heating at variant spatial frequencies for a porous MHD free convection system considering Cu-Al_2O_3/water hybrid nanoliquid. The governing equations are introduced utilizing a classical square cavity. Sheremet et al. [25] carried out the case of MHD free convection inside a wavy open porous tall cavity filled with a Cu-water nanofluid in the presence of an isothermal corner heater numerically.

Due to our knowledge, the authors neglected the case of Cattaneo–Christov heat flux impacts in their contributions of the hybrid nanofluids through cavities due to the complexity of the mathematical formulations. Therefore, this study aims to cover this gape. Moreover, there are a few contributions concerned with the applications in the wavy container, thus the intention behind the present analysis is to assay Cattaneo–Christov heat flux pattern with the influence of slant magnetic field. In addition, the substantial intention of the present contribution is to examine the numerical analysis of the natural convection heat flux paradigm implementing local thermal nonequilibrium on sinusoidal wavy cavity filled with Al_2O_3-Cu/water hybrid nanofluid under the impact of the internal heat generation, slant magnetic field and thermal radiation. The calculated outcomes are validated with early numerical published data and the impact of the significant factors and presented via graphically in the form of streamlines, isotherms, local and average Nusselt numbers.

2 Physical configuration

Figure 1 portrays the physical configuration of steady two-dimensional radiative natural convection heat transfer problem inside a wavy container with wall length H and undulation number λ and containing various types of the obstacles. The worked hybrid nanofluid undergoes Newtonian, laminar and incompressible flow. A nonvariable slant magnetic field of intensity B_0 is imposed of an inclination angle Ω. The walls of inner obstacles are kept at a cold temperature T_c. Furthermore, the feature of viscous dissipation has been ignored. Left and right walls are kept with temperature T_c, whilst the above and bellow walls are presumed as adiabatic and all wall are supposed to be impermeable. The porous medium, nano-size elements and regular fluid are given homogeneous and in thermal equilibrium. Thermophysical attributes and its values of alumina, copper and water used here are stated in Table 1. Besides, due to Rosseland approximation, radiation heat flux within the hybrid nanofluid porous container is imposed. The Boussinesq approximation is adopted for our governing flow equations [2, 13]

$$\frac{\partial u}{\partial x} + \frac{\partial v}{\partial y} = 0,$$

$$\begin{aligned}\frac{\rho_\mathrm{hnf}}{\varepsilon^2}\left(u\frac{\partial u}{\partial x} + v\frac{\partial u}{\partial y}\right) &= -\frac{\partial \tilde{P}}{\partial x} + \frac{\mu_\mathrm{hnf}}{\varepsilon}\left(\frac{\partial^2 u}{\partial x^2} + \frac{\partial^2 u}{\partial y^2}\right) - \frac{\mu_\mathrm{hnf}}{\tilde{K}}u \\ &\quad + g(\rho\beta)_\mathrm{hnf}(T_\mathrm{f} - T_\mathrm{c})\sin\gamma \\ &\quad + \sigma_{hnf}B_0^2\bigl(v\sin\Omega\cos\Omega - u\sin^2\Omega\bigr),\end{aligned} \tag{1}$$

$$\begin{aligned}\frac{\rho_\mathrm{hnf}}{\varepsilon^2}\left(u\frac{\partial v}{\partial x} + v\frac{\partial v}{\partial y}\right) &= -\frac{\partial \tilde{P}}{\partial y} + \frac{\mu_\mathrm{hnf}}{\varepsilon}\left(\frac{\partial^2 v}{\partial x^2} + \frac{\partial^2 v}{\partial y^2}\right) - \frac{\mu_\mathrm{hnf}}{\tilde{K}}v \\ &\quad + g(\rho\beta)_\mathrm{hnf}(T_\mathrm{f} - T_\mathrm{c})\cos\gamma \\ &\quad + \sigma_{hnf}B_0^2\bigl(u\sin\Omega\cos\Omega - v\cos^2\Omega\bigr),\end{aligned} \tag{2}$$

$$\begin{aligned}(\rho c_\mathrm{p})_\mathrm{hnf}\left(u\frac{\partial T_\mathrm{f}}{\partial x} + v\frac{\partial T_\mathrm{f}}{\partial y}\right) &= \varepsilon k_\mathrm{hnf}\left(\frac{\partial^2 T_\mathrm{f}}{\partial x^2} + \frac{\partial^2 T_\mathrm{f}}{\partial y^2}\right) + h_\mathrm{fs}(T_\mathrm{s} - T_\mathrm{f}) + \tilde{Q} \\ &\quad - \varepsilon\Lambda(\rho c_\mathrm{p})_\mathrm{hnf}\biggl\{u\frac{\partial u}{\partial x}u\frac{\partial T_\mathrm{f}}{\partial x} + v\frac{\partial v}{\partial y}\frac{\partial T_\mathrm{f}}{\partial y} + u^2\frac{\partial^2 T_\mathrm{f}}{\partial x^2} \\ &\quad + v^2\frac{\partial^2 T_\mathrm{f}}{\partial y^2} + 2uv\frac{\partial^2 T_\mathrm{f}}{\partial x\partial y} + u\frac{\partial v}{\partial x}\frac{\partial T_\mathrm{f}}{\partial y} + v\frac{\partial u}{\partial y}\frac{\partial T_\mathrm{f}}{\partial x}\biggr\},\end{aligned} \tag{3}$$

$$(1-\varepsilon)\left(k_\mathrm{s} + \frac{16\sigma^* T_\mathrm{c}^3}{3k^*}\right)\left(\frac{\partial^2 T_\mathrm{f}}{\partial x^2} + \frac{\partial^2 T_\mathrm{f}}{\partial y^2}\right) + h_\mathrm{fs}(T_\mathrm{f} - T_\mathrm{s}) + (1-\varepsilon)\tilde{Q} = 0. \tag{4}$$

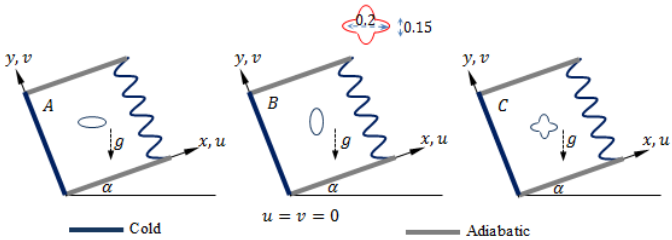

Figure 1. Schematically of the physical model of the porous cavity.

Table 1. Thermophysical attributes of water, copper and alumina [11, 13].

Property	H_2O	Cu	Al_2O_3
ρ	997.1	8933	3970
c_p	4179	385	765
k	0.613	401	40
β	$21 \cdot 10^{-5}$	$1.67 \cdot 10^{-5}$	$0.85 \cdot 10^{-5}$
σ	0.05	$5.96 \cdot 10^{7}$	$1 \cdot 10^{-10}$

The proper boundary conditions for the porous container on the left wall, the right wall, the top wall, the bottom wall and over the inner obestical considered as follows, respectively:

$$\begin{aligned}
&u = v = 0, \quad T_\mathrm{f} = T_\mathrm{c} = T_\mathrm{s}, \quad x = 0,\ 0 \leqslant y \leqslant H,\\
&u = v = 0, \quad T_\mathrm{f} = T_\mathrm{c} = T_\mathrm{s}, \quad x = H - AH\left(1 - \frac{\cos 2\pi\lambda y}{H}\right),\ 0 \leqslant y \leqslant H,\\
&u = v = 0, \quad \frac{\partial T_\mathrm{f}}{\partial y} = \frac{\partial T_\mathrm{s}}{\partial y} = 0, \quad 0 \leqslant x \leqslant H,\ y = H,\\
&u = v = 0, \quad \frac{\partial T_\mathrm{f}}{\partial y} = \frac{\partial T_\mathrm{s}}{\partial y} = 0, \quad 0 \leqslant x \leqslant H,\ y = 0,\\
&T_\mathrm{f} = T_\mathrm{s} = T_\mathrm{c},
\end{aligned}$$

where notations appearing in governing flow Eqs. (2)–(4) are as follows: x and y stand for Cartesian coordinates scaled along the vertical and horizontal walls of the container, respectively; u and v symbolize the hybrid nanofluid velocities along the x- and y- axes, respectively; T denotes the hybrid nanofluid temperature, P indicates the hybrid nanofluid pressure, g indicates the gravity acceleration, K means the permeability and $\tilde{Q}$ means the volumetric heat generation/absorption rate.

The concerned factors of the Cu, Al_2O_3 and water hybrid nanoliquid, i.e., viscosity, density, electrical conductivity, thermal conductivity, heat capacity and effective electrical conductivity are defined as [11, 13, 14]

$$\mu_\mathrm{hnf} = \frac{\mu_\mathrm{nf}}{(1-\varphi_2)^{2.5}}, \qquad \mu_\mathrm{nf} = \frac{\mu_\mathrm{bf}}{(1-\varphi_1)^{2.5}},$$

$$\rho_\mathrm{hnf} = (1-\varphi_2)\rho_\mathrm{nf} + \varphi_2\rho_2, \qquad \rho_\mathrm{nf} = (1-\varphi_1)\rho_\mathrm{bf} + \varphi_1\rho_1,$$

$$(\rho c_p)_{\mathrm{hnf}} = (1-\varphi_2)(\rho c_p)_{\mathrm{nf}} + \varphi_2(\rho c_p)_2, \qquad (\rho c_p)_{\mathrm{nf}} = (1-\varphi_1)(\rho c_p)_{\mathrm{bf}} + \varphi_1(\rho c_p)_1,$$
$$(\rho\beta)_{\mathrm{hnf}} = (1-\varphi_2)(\rho\beta)_{\mathrm{nf}} + \varphi_2(\rho\beta)_2, \qquad (\rho\beta)_{\mathrm{nf}} = (1-\varphi_1)(\rho\beta)_{\mathrm{bf}} + \varphi_1(\rho\beta)_1,$$
$$\frac{k_{\mathrm{hnf}}}{k_{\mathrm{nf}}} = \frac{(k_2+2k_{\mathrm{nf}}) - 2\varphi_2(k_{\mathrm{nf}}-k_2)}{(k_2+2k_{\mathrm{nf}}) + \varphi_2(k_{\mathrm{nf}}-k_2)}, \qquad \frac{k_{\mathrm{nf}}}{k_{\mathrm{bf}}} = \frac{(k_1+2k_{\mathrm{bf}}) - 2\varphi_1(k_{\mathrm{bf}}-k_1)}{(k_1+2k_{\mathrm{bf}}) + \varphi_1(k_{\mathrm{bf}}-k_1)},$$
$$\frac{\sigma_{\mathrm{hnf}}}{\sigma_{\mathrm{nf}}} = \frac{(\sigma_2+2\sigma_{\mathrm{nf}}) - 2\varphi_2(\sigma_{\mathrm{nf}}-\sigma_2)}{(\sigma_2+2\sigma_{\mathrm{nf}}) + \varphi_2(\sigma_{\mathrm{nf}}-\sigma_2)}, \qquad \frac{\sigma_{\mathrm{nf}}}{\sigma_{\mathrm{bf}}} = \frac{(\sigma_1+2\sigma_{\mathrm{bf}}) - 2\varphi_1(\sigma_{\mathrm{bf}}-\sigma_1)}{(\sigma_1+2\sigma_{\mathrm{bf}}) + \varphi_1(\sigma_{\mathrm{bf}}-\sigma_2)},$$

where $\varphi_1 = \varphi_{\mathrm{Al_2O_3}}$ and $\varphi_2 = \varphi_{\mathrm{Cu}}$. With the help of the dimensionless scales

$$(x,y) = (X,Y)H, \qquad (u,v) = (U,V)\frac{\alpha_{\mathrm{f}}}{H}, \qquad P = \frac{\tilde{P}H^2}{\rho_{\mathrm{f}}\alpha_{\mathrm{f}}^2}, \qquad \theta = \frac{T-T_{\mathrm{c}}k_{\mathrm{f}}}{\tilde{Q}H^2}$$

and using Eqs. (2)–(4), then the altered dimensionless flow equations are

$$\frac{\partial U}{\partial X} + \frac{\partial V}{\partial Y} = 0,$$
$$\begin{aligned}\frac{1}{\varepsilon^2}\left(U\frac{\partial U}{\partial X} + V\frac{\partial U}{\partial Y}\right) = {}& -\frac{\partial P}{\partial X} + \frac{Pr}{\varepsilon}\frac{\nu_{\mathrm{hnf}}}{\nu_{\mathrm{f}}}\left(\left(\frac{\partial^2 U}{\partial X^2} + \frac{\partial^2 U}{\partial Y^2}\right) - \frac{\varepsilon}{K}U\right)\\ &+ \frac{\beta_{\mathrm{hnf}}}{\beta_{\mathrm{f}}}Ra\,Pr\,\theta_{\mathrm{f}}\sin\gamma\\ &+ \frac{\rho_{\mathrm{f}}}{\rho_{\mathrm{hnf}}}\frac{\sigma_{\mathrm{hnf}}}{\varepsilon\sigma_{\mathrm{f}}}Ha^2 Pr\big(V\sin\Omega\cos\Omega - U\sin^2\Omega\big),\end{aligned}$$
$$\begin{aligned}\frac{1}{\varepsilon^2}\left(U\frac{\partial V}{\partial X} + V\frac{\partial V}{\partial Y}\right) = {}& -\frac{\partial P}{\partial Y} + \frac{Pr}{\varepsilon}\frac{\nu_{\mathrm{hnf}}}{\nu_{\mathrm{f}}}\left(\left(\frac{\partial^2 V}{\partial X^2} + \frac{\partial^2 V}{\partial Y^2}\right) - \frac{\varepsilon}{K}V\right)\\ &+ \frac{\beta_{\mathrm{hnf}}}{\beta_{\mathrm{f}}}Ra\,Pr\,\theta_{\mathrm{f}}\cos\gamma\\ &+ \frac{\rho_{\mathrm{f}}}{\rho_{\mathrm{hnf}}}\frac{\sigma_{\mathrm{hnf}}}{\varepsilon\sigma_{\mathrm{f}}}Ha^2 Pr\big(U\sin\Omega\,\cos\Omega - V\cos^2\Omega\big),\end{aligned}$$
$$\begin{aligned}\frac{(\rho c_{\mathrm{p}})_{\mathrm{hnf}}}{(\rho c_{\mathrm{p}})_{\mathrm{f}}}\left(U\frac{\partial\theta_{\mathrm{f}}}{\partial X} + V\frac{\partial\theta_{\mathrm{f}}}{\partial Y}\right) = {}& \varepsilon\frac{k_{\mathrm{hnf}}}{k_{\mathrm{f}}}\left(\frac{\partial^2\theta_{\mathrm{f}}}{\partial X^2} + \frac{\partial^2\theta_{\mathrm{f}}}{\partial Y^2}\right) + H^*(\theta_{\mathrm{s}} - \theta_{\mathrm{f}}) + Q\\ &- \varepsilon\delta\left\{U\frac{\partial U}{\partial X}\frac{\partial\theta_{\mathrm{f}}}{\partial X} + V\frac{\partial V}{\partial Y}\frac{\partial\theta_{\mathrm{f}}}{\partial Y} + U^2\frac{\partial^2\theta_{\mathrm{f}}}{\partial X^2} + V^2\frac{\partial^2\theta_{\mathrm{f}}}{\partial Y^2}\right.\\ &\left. + 2UV\frac{\partial^2\theta_{\mathrm{f}}}{\partial X\partial Y} + U\frac{\partial V}{\partial X}\frac{\partial\theta_{\mathrm{f}}}{\partial Y} + V\frac{\partial U}{\partial Y}\frac{\partial\theta_{\mathrm{f}}}{\partial X}\right\},\end{aligned}$$
$$(1+Rd)\left(\frac{\partial^2\theta_{\mathrm{f}}}{\partial X^2} + \frac{\partial^2\theta_{\mathrm{f}}}{\partial Y^2}\right) + K_r H^*(\theta_{\mathrm{f}} - \theta_{\mathrm{s}}) + k_{\mathrm{fs}}Q = 0.$$

Due to the previous equations, the concerned factors are formulated as

$$Pr = \frac{(\mu c_p)_{\mathrm{f}}}{k_{\mathrm{f}}}, \qquad Ra = \frac{g(\rho\beta)_{\mathrm{f}}(\rho c_p)_{\mathrm{f}}H^5\tilde{Q}}{\mu_{\mathrm{f}}k_{\mathrm{f}}^2}, \qquad \delta = \frac{k_{\mathrm{f}}\varLambda}{H^2(\rho c_p)_{\mathrm{f}}},$$

$$Ha^2 = B_0^2 H^2\left(\frac{\sigma_\mathrm{f}}{\mu_\mathrm{f}}\right), \qquad Da = \frac{K}{H^2}, \qquad Kr = \frac{k_\mathrm{c} H^2}{\nu_\mathrm{f}} Rd = \frac{16\sigma^* T_c^3}{3k^* k_\mathrm{f}}.$$

Once again, the imposed boundary conditions on the left wall, the right wall, the top wall, the bottom wall and the inner obestical altered into, respectively,

$$\begin{aligned}
&U = V = 0, \quad \theta_\mathrm{f} = \theta_\mathrm{s}, \quad x = 0,\ 0 \leqslant Y \leqslant 1,\\
&U = V = 0, \quad \theta_\mathrm{f} = \theta_\mathrm{s}, \quad X = 1 - A(1-\cos 2\pi\lambda Y),\ 0 \leqslant Y \leqslant 1,\\
&U = V = 0, \quad \frac{\partial\theta_\mathrm{f}}{\partial Y} = \frac{\partial\theta_\mathrm{s}}{\partial Y = 0}, \quad 0 \leqslant X \leqslant 1,\ y = 1,\\
&U = V = 0, \quad \frac{\theta_\mathrm{f}}{\partial Y} = \frac{\partial\theta_\mathrm{s}}{\partial Y = 0}, \quad 0 \leqslant x \leqslant 1,\ y = 0,\\
&\theta_\mathrm{f} = \theta_\mathrm{s} = 0.
\end{aligned}$$

The local and average Nusselt numbers are evaluated by

$$Nu_\mathrm{v} = -\frac{k_\mathrm{hnf}}{k_\mathrm{f}}\frac{\partial\theta_\mathrm{f}}{\partial n}, \qquad Nu_\mathrm{mf} = \frac{1}{L_\mathrm{w}}\int_0^{L_\mathrm{w}} Nu_\mathrm{v}\,\mathrm{d}L_\mathrm{w}.$$

Also, the local and average Nusselt numbers of the solid can be written as

$$Nu_\mathrm{ss} = -(1+Rd)\frac{\partial\theta_\mathrm{s}}{\partial n}, \qquad Nu_\mathrm{ms} = \frac{1}{L_\mathrm{w}}\int_0^{L_\mathrm{w}} Nu_\mathrm{ss}\,\mathrm{d}L_\mathrm{w}.$$

3 Solution approach

To solve the aforementioned system of equations, the nonorthogonal control volume described by Patankar [19] is applied. This methodology starts with introducing the new coordinates ξ_1 and ξ_2 as

$$\xi_1 = \frac{X - g_1(Y)}{\Delta(Y)}, \qquad \xi_2 = Y,$$

where

$$\begin{gathered}
g_1(Y) = 0, \qquad g_2(Y) = 1 - A\bigl(1-\cos(2\pi\lambda Y)\bigr),\\
\Delta(Y) = g_2(Y) - g_1(Y) = 1 - A\bigl(1-\cos(2\pi\lambda Y)\bigr).
\end{gathered}$$

Then the system of the governing equations can be expressed by the following general forms:

$$\frac{\partial}{\partial X_j}[U_j\Omega^*] = \frac{\partial}{\partial X_j}\left[\Gamma\frac{\partial\Omega^*}{\partial X_j}\right] + S_{\Omega^*}.$$

Here the chain rule is used to estimate the first derivatives with respect to $X_1 = X$ and $X_2 = Y$:

$$\begin{bmatrix}\frac{\partial\Omega^*}{\partial X_1}\\ \frac{\partial\Omega^*}{\partial X_2}\end{bmatrix} = \frac{1}{J}\begin{bmatrix}\beta_{11} & \beta_{12}\\ \beta_{21} & \beta_{22}\end{bmatrix}\begin{bmatrix}\frac{\partial\Omega^*}{\partial\xi_1}\\ \frac{\partial\Omega^*}{\partial\xi_2}\end{bmatrix}. \tag{5}$$

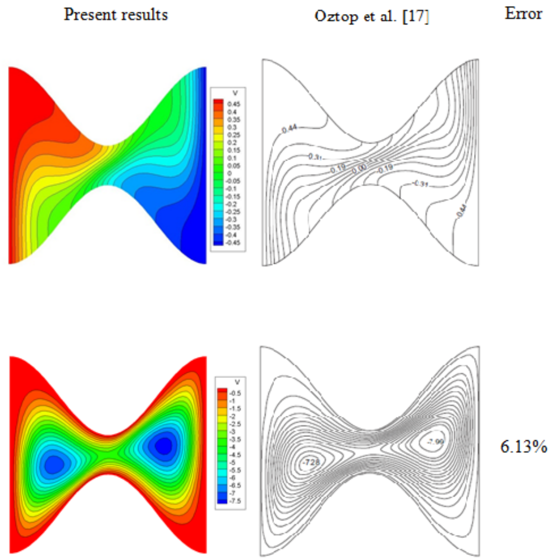

Figure 2. Validation test at $Ra_E = Ra_l = 10^5$, $a = 0.8$.

In Eq. (5), β_{11}, β_{12}, β_{21}, β_{22} and J are given by

$$\beta_{11} = \frac{\partial X_2}{\partial \xi_2}, \qquad \beta_{12} = -\frac{\partial X_2}{\partial \xi_1}, \qquad \beta_{21} = -\frac{\partial X_1}{\partial \xi_2}, \qquad \beta_{22} = \frac{\partial X_1}{\partial \xi_1},$$
$$J = \beta_{11}\beta_{22} - \beta_{12}\beta_{21}.$$

The previous transformations is applied to approximate the convective terms as

$$U_j \frac{\partial \Omega^*}{\partial X_j} = \frac{1}{J} \frac{\partial}{\partial X_i} \big[\hat{U}_k \Omega^*\big].$$

Here $[\hat{U}_k]$ is the converted velocities ($\hat{U}_k = U_j \beta_{jk}$). Additionally, the diffusive terms are given by

$$\frac{\partial}{\partial X_j} \left[\Gamma \frac{\partial \Omega^*}{\partial X_j}\right] = \frac{1}{J} \frac{\partial}{\partial \xi_i} \left[\frac{\Gamma}{J} \beta_{ik} \frac{\partial \Omega^*}{\partial \xi_k}\right], \tag{6}$$

where $\beta_{ik} = \beta_{ji}\beta_{jk}$. Furthermore, an algebraic system of equations is obtained. This system is solved iteratively using ADI algorithm. A home FORTRAN code is performed to implement this technique, and the convergence criterion is 10^{-6}. Regarding the grid size, it is noted that the grid 81×81 and 101×101 are enough for all the calculations. Figure 2 shows the validation test with the similar shape (wavy enclosure). A comparison with the results presented by Oztop et al. [17] is carried out. It is remarkable that the streamlines and isotherms are almost the same, and the relative error between the values of the maximum stream function is 6.13%.

4 Results and discussion

This section presents a comprehensive discussion of the obtained results. Here the illustration tools of the results are contours of the streamlines, isotherms for the fluid phase and isotherms for the solid phase. The controlling parameters are varied in wide ranges, namely, the thermal relaxation parameter δ ($0 \leqslant \delta \leqslant 10$), various locations of the inner shape $(X, Y) = (0.25, 0.5), (0.75, 0.5), (0.5, 0.25)$ and $(0.5, 0.75)$, the radiation parameter Rd ($0 \leqslant Rd \leqslant 20$), the Hartmann number Ha ($0 \leqslant Ha \leqslant 100$), the heat transfer coefficient H^* ($0 \leqslant H^* \leqslant 20$), the heat generation parameter Q ($0.25 \leqslant Q \leqslant 3$) and the undulation number λ ($1 \leqslant \lambda \leqslant 5$). In all the obtained results the hybrid nanofluid case is applied with $\varphi_1 = \varphi_2 = 0.05$.

Figure 3 demonstrates the contours of streamlines, isotherms of fluid phase and isotherms of solid phase for the variations of the relaxation parameter δ at $Ha = 10$, $Q = 1$, $\varepsilon = 0.5$, $H^* = 10$, $Rd = 0.5$. This figure is performed using case C (cross-shaped ellipse). Also, the range of δ is between 0 and 10. Two convective cells are performed within the domain for all values of δ. Additionally, the increasing values of δ cause a clearly enhancement in the rate of the hybrid nanofluids flow. The isotherms for the fluid and porous phases revealed that there are heated zones near the horizontal walls and cold zones near the cold boundaries. The increase in δ results in an increase in the thermal zones together with the maximum temperature. These behaviors are due to the additionally heat flux (Cattaneo–Christov heat flux), which enhance the temperature differences, and hence the convective flow is augmented.

Features of the streamlines, fluid-phase temperature and solid-phase temperature for various locations of the inner obstructs at $Ha = 10$, $Q = 1$, $\varepsilon = \delta = 0.5$, $H^* = 10$, $Rd = 0.5$ are shown in Fig. 4. Here cross-shaped ellipse are used (case C), and five locations are tested, namely, $(0.25, 0.5), (0.75, 0.5), (0.5, 0.25), (0.5, 0.75), (0.5, 0.5)$. Various configurations for the flow and thermal features are noted as the locations are changed. Here the isotherms and streamlines features are gathered in the opposite direction to the cross-shaped ellipse. The natural convection flow and heat transfer get their maximum at the location $(0.75, 0.5)$ comparing with the other considered locations. Also, the temperature gradients get their minimum in the location $(0.25, 0.5)$.

Wide ranges of the radiation parameter Rd ($0 \leqslant Rd \leqslant 20$) and the Hartmann number Ha ($0 \leqslant Ha \leqslant 100$) are considered. The impacts of these ranges on the streamlines, temperature for the fluid and porous phases at $Q = 1$, $\varepsilon = \delta = 0.5$, $H^* = 10$ using cases C and Bare depicted in Figs. 5 and 6. Here it should be mentioned that the features of θ_s are closed to those of θ_f due to the higher heat transfer coefficient $H^* = 10$. The convective transport is enhanced as Rd is maximizing, and hence the flow and temperature distributions are augmented as Rd is increased. Physically, these behaviors return to the additional heat generation resulting from the radiation flux, and hence the buoyancy force is enhanced. On the contrary, the considered range of Ha causes a reduction in the flow rate and temperature features. These behaviors are due to the Lorentz force, which works against the convective transport.

Figures 7(a)–7(c) disclose the profiles of the fluid-phase Nusselt number Nu_{v} for the variations of the relaxation parameter δ, various locations of the inner obstructs and heat

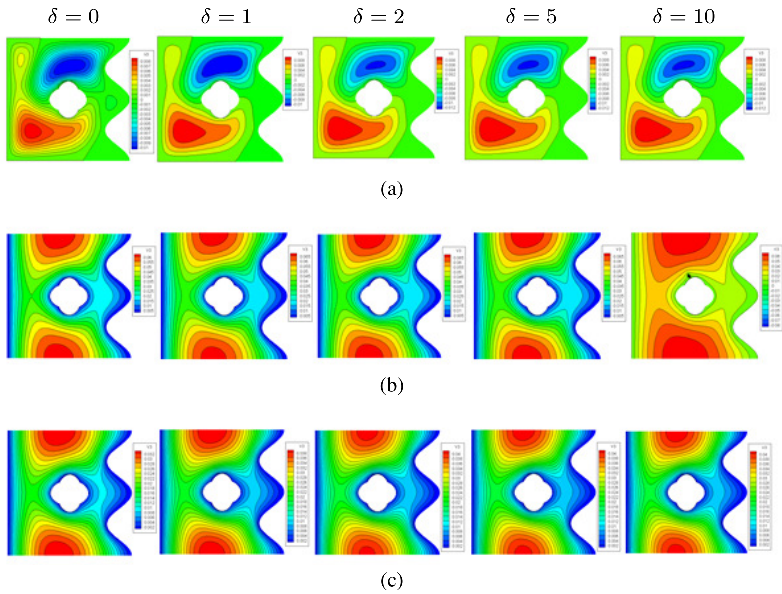

Figure 3. Contours of streamlines (a) isotherms of fluid phase (b) and isotherms of solid phase (c). Case C for Al_2O_3-Cu/water hybrid nanofluid at $Ha = 10$, $Q = 1$, $\varepsilon = 0.5$, $H^* = 10$, $Rd = 0.5$.

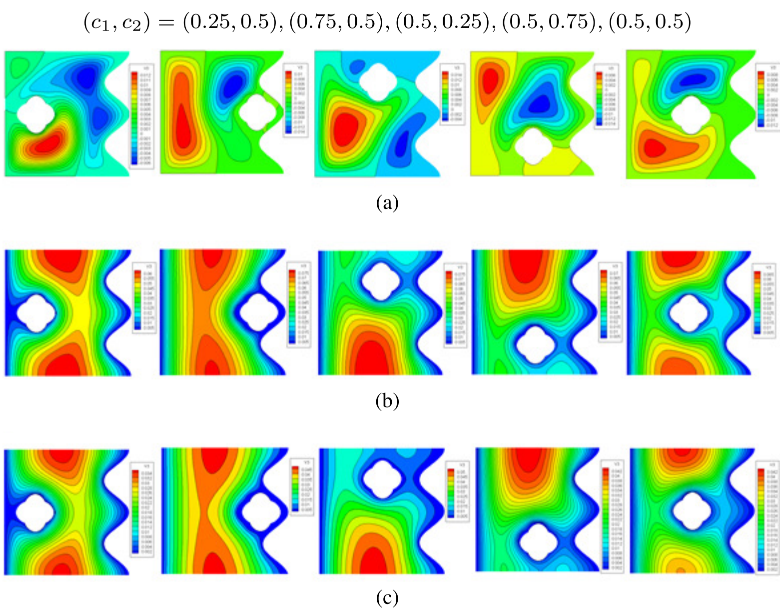

Figure 4. Contours of streamlines (a) isotherms of fluid phase (b) and isotherms of solid phase (c). Case C for Al_2O_3-Cu/water hybrid nanofluid at $Ha = 10$, $Q = 1$, $\varepsilon = 0.5$, $\delta = 0.5$, $H^* = 10$.

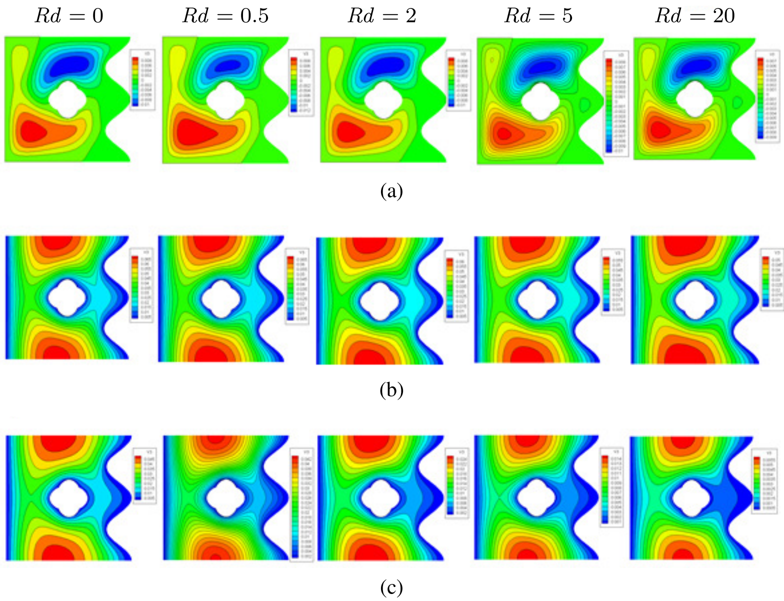

Figure 5. Contours of streamlines (a) isotherms of fluid phase (b) and isotherms of solid phase (c). Case C for Al_2O_3-Cu/water hybrid nanofluid at $Ha = 10$, $Q = 1$, $\varepsilon = 0.5$, $\delta = 0.5$, $H^* = 10$.

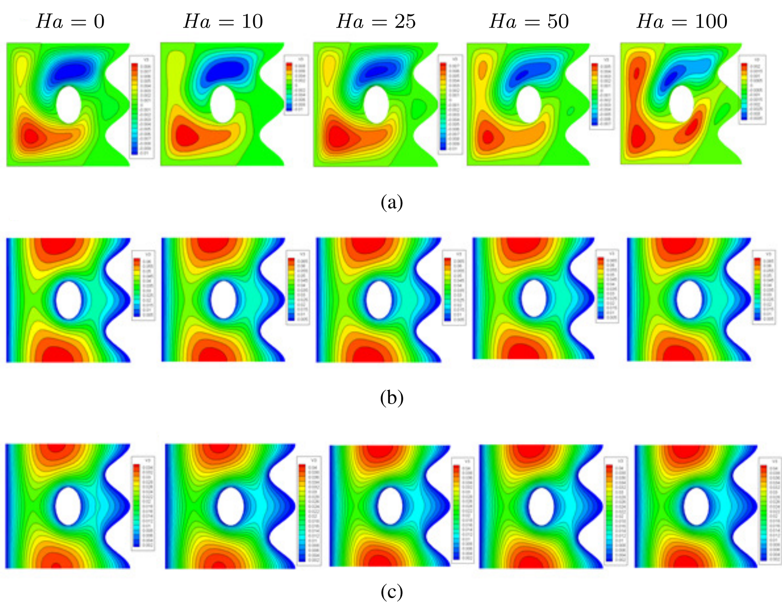

Figure 6. Contours of streamlines (a) isotherms of fluid phase (b) and isotherms of solid phase (c). Case B for Al_2O_3-Cu/water hybrid nanofluids at $Q = 1$, $\varepsilon = 0.5$, $\varepsilon = 0.5$, $H^* = 10$, $Rd = 0.5$, $\delta = 0.5$.

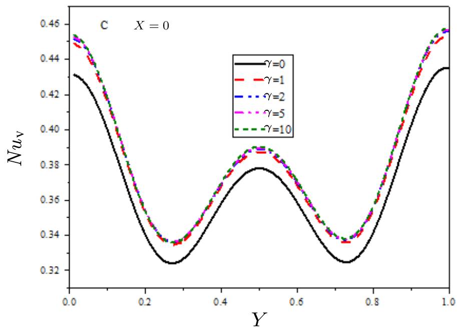

(a) $H^* = 10,\ Rd = 0.5$.

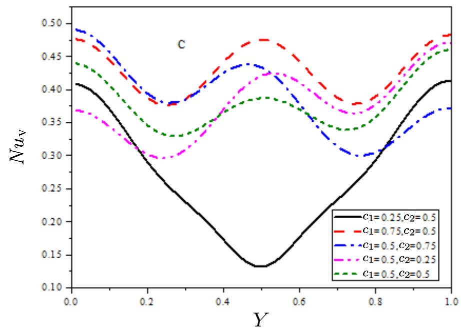

(b) $\delta = 0.5,\ H^* = 10$.

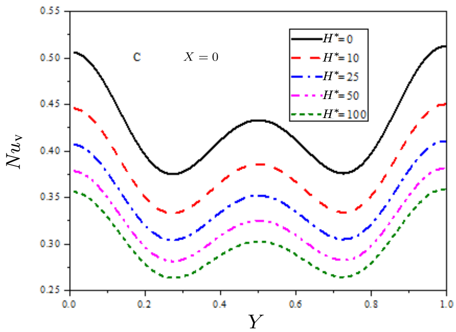

(c) $\delta = 0.5,\ Rd = 0.5$.

Figure 7. Profiles of the local Nusselt number of fluid phase for Al_2O_3-Cu/water hybrid nanofluid at $Ha = 10$, $Q = 1$, $\varepsilon = 0.5$.

transfer coefficient H^* at $Q = 1$, $\varepsilon = Rd = 0.5$. It is remarkable that the features of Nu_v follow the wavy geometry of the enclosure side wall. Also, the maximizing of δ is better to obtain a higher rate of the heat transfer. Unlike the impact of δ, the minimizing of the heat transfer coefficient H^* causes a higher rate of the heat transfer between the fluid and porous phases, which leads to the reduction of the heat transfer rate between the fluid and side wall. Additionally, the second location of the inner shape $(0.75, 0.5)$ gives the higher values of Nu_v, while the Nu_v takes their minimum values at the location $(0.25, 0.5)$. In a related context, two graphical illustrations are presented in Fig. 8 to display the significance of the radiation parameter Rd on both the local Nusselt number for the fluid Nu_v and solid phases Nu_ss at $Ha = 10$, $Q = 1$, $\varepsilon = \delta = 0.5$, $H^* = 10$. It is noted that the growing in Rd results in a raising in the solid-phase temperature gradients, and hence Nu_ss is augmented. On the contrary, Nu_v is minimizing as Rd is increases due to the lower convective flow.

Figures 9 and 10 depict the average Nusselt coefficients for the fluid Nu_mf and for the solid Nu_ms under the impacts of the heat generation/absorption parameter Q, undulation number λ and NP (nanoparticles) volume fraction φ at $Ha = 10$, $Q = 1$, $\varepsilon = \delta = 0.5$,

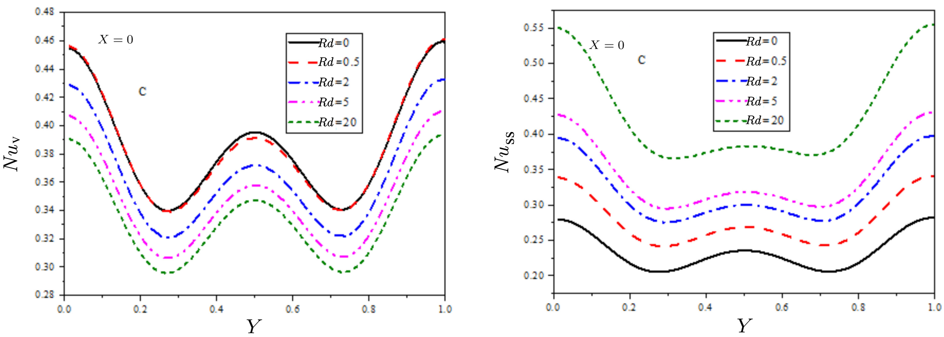

(a) (b)

Figure 8. Profiles of the local Nusselt number of fluid phase (a), and solid phase (b) for Al_2O_3-Cu/water hybrid nanofluid at $Ha = 10$, $Q = 1$, $\varepsilon = 0.5$, $\delta = 0.5$, $H^* = 10$.

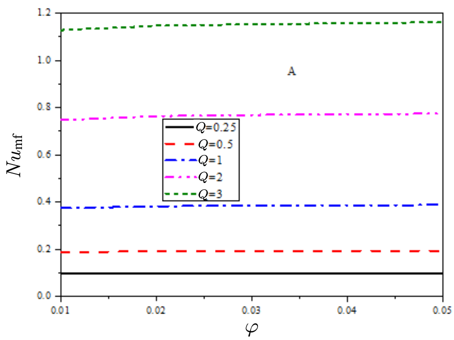

Figure 9. Variation of the average Nusselt number of fluid phase for Al_2O_3-Cu/water hybrid nanofluid at $Ha = 10$, $\varepsilon = 0.5$, $H^* = 10$, $Rd = 0.5$, $\delta = 0.5$.

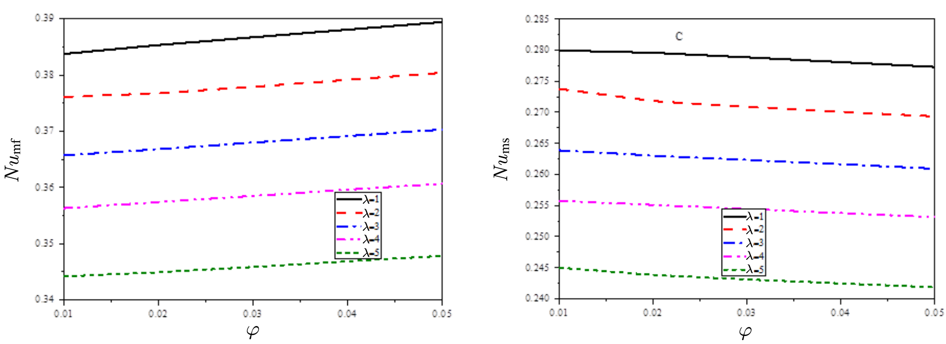

(a) (b)

Figure 10. Variation of the average Nusselt number of fluid phase (a) and solid phase (b) for Al_2O_3-Cu/water hybrid nanofluid at $Ha = 10$, $Q = 1$, $\varepsilon = 0.5$, $\delta = 0.5$, $H^* = 10$.

$H^* = 10$. The figures revealed that a clear rising in Nu_{mf} as either Q or φ is growing. Here the increase in Q means a good buoyancy-driven flow and hence Nu_{mf}. Also, the increase in φ refers to a good thermal conductivity of the mixture, and hence rate of the heat transfer is augmented. On the other side, the rising in λ increases the complexity of the geometry, and hence both of Nu_{mf} and Nu_{ms} are diminishing.

5 Conclusions

The magnetohydrodynamics convective transport within a wavy porous cavity filled with hybrid nanofluids (Al_2O_3-Cu-H_2O) has been studied. Cattaneo–Christov heat flux together with the radiation and heat generation/absorption were considered. Various shapes of the inner obstructs were used to control the flow, and the LTNE conditions between the fluid and solid phases was assumed. Two different inclination angles were introduced for the flow domain and magnetic field. The nonorthogonal FVM technique was applied to solve the governing system. The following major outcomes can be pointed out:

- Cattaneo–Christov heat flux enhances the convective flow and rate of the heat transfer.
- The radiation flux enhances Nu_{ss}, while it has negative impacts on Nu_{v}.
- The maximizing of the NP concentration is better to get a higher rate of the heat transfer.
- The flow features can be well control using various locations of the inner shape.
- The location $(0.75, 0.5)$ is better for the rate of the flow and temperature gradients.
- The profiles of solid-phase temperature are closed to the those of the fluid-phase temperature at the higher values of H^*.

In addition, this study can be extended in the future to include the case of a variable magnetic field, non-Newtonian nanofluids or phase change materials case.

References

1. S.E. Ahmed, Non-Darcian natural convection of a nanofluid due to triangular fins within trapezoidal enclosures partially filled with a thermal non-equilibrium porous layer, *J. Therm. Anal. Calorim.*, **145**(2):1–16, 2020, https://doi.org/10.1007/s10973-020-09831-4.

2. S.E. Ahmed, M.A. Mansour, A.M. Rashad, Z. Morsy, MHD Fee convection and sinusoidal heating in a wavy cavity filled with a heat-generating porous medium using Cu-water nanofluids, *Comput. Therm. Sci.*, **12**(3):217–232, 2020, https://doi.org/10.1615/ComputThermalScien.2020030316.

3. N. Biswas, D.K. Mandal, N.K. Manna, R.S.R. Gorla, A.J. Chamkha, Magnetohydrodynamic thermal characteristics of water-based hybrid nanofluid filled non-Darcian porous wavy enclosure: effect of undulation, *Int. J. Numer. Methods Heat Fluid Flow*, **32**(5):1742–1777, 2021, https://doi.org/10.1108/HFF-03-2021-0190.

4. N. Biswas, U.K. Sarkar, A.J. Chamkha, N.K. Manna, Magneto-hydrodynamic thermal convection of $CuAl_2O_3$/water hybrid nanofluid saturated porous media subjected to half-

sinusoidal nonuniform heating, *J. Therm. Anal. Calorim.*, **143**:1727–1753, 2021, https://doi.org/10.1007/s10973-020-10123-0.

5. A. Chamkha, M. Ismael, A. Kasaeipoor, T. Armaghani, Entropy generation and natural convection of CuO-Water nano uid in C-shaped cavity under magnetic field, *Entropy*, **50**:1–18, 2016, https://doi.org/10.3390/e18020050.
6. J.M. House, C. Beckermann, T.F. Smith, Effect of a centered conducting body on natural convection heat transfer in an enclosure, *Numer. Heat Transfer, Part A*, **18**:213–225, 1990, https://doi.org/10.1080/10407789008944791.
7. M.D. Ikram, M.I. Asjad, A. Akgu, D. Baleanu, Effects of hybrid nanofluid on novel fractional model of heat transfer flow between two parallel plates, *Alexandria Eng. J.*, **60**:3595–3604, 2021, https://doi.org/10.1016/j.aej.2021.01.054.
8. G.H.R. Kefayati, Simulation of heat transfer and entropy generation of MHD natural convection of non-Newtonian nanofluid in an enclosure, *Int. J. Heat Mass Transfer*, **92**:1066–1089, 2016, https://doi.org/10.1016/J.IJHEATMASSTRANSFER.2015.09.078.
9. S.U. Khan, S.A. Shehzad, Brownian movement and thermophoretic aspects in third grade nanofluid over oscillatory moving sheet, *Phys. Scr.*, **94**(9):095202, 2019, https://doi.org/10.1088/1402-4896/ab0661.
10. D. Madhesh, R. Parameshwaran, S. Alaiselvam, Experimental investigation on convective heat transfer and rheological characteristics of Cu-TiO_2 hybrid nanofluids, *Exp. Therm. Fluid Sci.*, **52**:104–115, 2014, https://doi.org/10.1016/j.expthermflusci.2013.08.026.
11. A. Mahdy, S.E. Ahmed, M.A. Mansour, Entropy generation for MHD natural convection in enclosure with a micropolar uid saturated porous medium with Al_2O_3-Cu water hybrid nanofluid, *Nonlinear Anal. Model. Control*, **26**(6):1123–1143, 2021, https://doi.org/10.15388/namc.2021.26.24940.
12. A.H. Mahmoudi, I. Pop, M. Shahi, Effect of magnetic field on natural convection in a triangular enclosure filled with nanofluid, *Int. J. Therm. Sci.*, **59**:126–140, 2012, https://doi.org/10.1016/j.ijthermalsci.2012.04.006.
13. M.A. Mansour, A. Mahdy, S.E. Ahmed, An inclined MHD mixed radiative-convection flow of a micropolar hybrid nanofluid within a lid-driven inclined odd-shaped cavity, *Phys. Scr.*, **96**(2):025705, 2021, https://doi.org/10.1088/1402-4896/abd1b0.
14. M.A. Mansour, A. Mahdy, S.E. Ahmed, An inclined mhd mixed radiative-convection ow of a micropolar hybrid nanofuid within a lid-driven inclined odd-shaped cavity, *Phys. Scr.*, **96**(2): 25705, 2021, https://doi.org/10.1088/1402-4896/abd1b0.
15. M. Muthtamilselvan, P. Kaswamy, J. Lee, Heat transfer enhancement of copper-water nanofluids in a lid-driven enclosure, *Commun. Nonlinear Sci. Numer. Simul.*, **15**(6):1501–1510, 2010, https://doi.org/10.1016/j.cnsns.2009.06.015.
16. S. Nadeem, N. Ullah, A.U. Khan, Impact of an oblique stagnation point on MHD micropolar nanomaterial in porous medium over an oscillatory surface with partial slip, *Phys. Scr.*, **94**(6):1–23, 2019, https://doi.org/10.1088/1402-4896/ab0b58.
17. H.F. Oztop, E. Abu-Nada, Y. Varol, A. Chamkha, Natural convection in wavy enclosures with volumetric heat sources, *Int. J. Therm. Sci.*, **50**(4):502–514, 2011, https://doi.org/10.1016/j.ijthermalsci.2010.10.015.

18. S. Parvin, R. Nasrin, Analysis of the flow and heat transfer characteristics for MHD free convection in an enclosure with a heated obstacle, *Nonlinear Anal. Model. Control*, **1**(1):59–72, 2011, https://doi.org/10.15388/NA.16.1.14117.
19. S. Patankar, *Numerical Heat Transfer and Fluid Flow*, CRC Precc, Boca Raton, FL, 1980, https://doi.org/10.1201/9781482234213.
20. I. Pop, M. Sheremet, D.S. Cimpean, Natural convection in a partially heated wavy cavity filled with a nanofluid using Buongiorno's nanofluid model, *Int. J. Numer. Methods Heat Fluid Flow*, **27**(4):924–940, 2017, https://doi.org/10.1108/HFF-12-2015-0529.
21. F. Selimefendigil, H.F. Oztop, Corrugated conductive partition effects on MHD free convection of CNT-water nanofluid in a cavity, *Int. J. Heat Mass Transfer*, **129**:265–277, 2019, https://doi.org/10.1016/J.IJHEATMASSTRANSFER.2018.09.101.
22. M. Sheikholeslami, Magnetic field influence on nanofluid thermal radiation in a cavity with tilted elliptic inner cylinder, *J. Mol. Liq.*, **229**:137–147, 2017, https://doi.org/10.1016/j.molliq.2016.12.024.
23. M. Sheikholeslami, H.B. Rokni, Magnetohydrodynamic CuO-water nanofluid in a porous complex shaped enclosure, *ASME J. Therm. Sci. Eng. Appl.*, **9**(4):041007, 2017, https://doi.org/10.1115/1.4035973.
24. M. Sheikholeslami, M. Sadoughi, Mesoscopic method for MHD nanofluid ow inside a porous cavity considering various shapes of nanoparticles, *Int. J. Heat Mass Transfer*, **113**:106–114, 2017, https://doi.org/10.1016/j.ijheatmasstransfer.2017.05.054.
25. M.A. Shereme, H.F. Oztop, I. Pop, K. Al-Salem, MHD free convection in a wavy open porous tall cavity filled with nanofluids under an effect of corner heater, *Int. J. Heat Mass Transfer*, **103**:955–964, 2016, https://doi.org/10.1016/j.ijheatmasstransfer.2016.08.006.
26. S.L. Sundar, M.K. Singh, A.C. Sousa, Enhanced heat transfer and friction factor of MWCNTFe_3O_4/water hybrid nanofluids, *Int. Commun. Heat Mass Transfer*, **52**:73–83, 2014, https://doi.org/10.1016/j.icheatmasstransfer.2014.01.012.
27. S. Suresh, K. Venkitaraj, P. Selvakumar, M. Chandrasekar, Synthesis of Al_2O_3-cu/water hybrid nanofluids using two step method and its thermo physical properties, *Colloids Surf. A*, **388**(1):41–48, 2011, https://doi.org/10.1016/j.colsurfa.2011.08.005.
28. M. Turkyilmazoglu, Cooling of particulate solids and fluid in a moving bed heat exchanger, *J. Heat Transfer*, **141**(11):114501–114505, 2019, https://doi.org/10.1115/1.4044590.
29. M. Usman, M. Hamid, T. Zubair, R.U. Haq, W. Wang, Cu-Al_2O_3/Water hybrid nanofluid through a permeable surface in the presence of nonlinear radiation and variable thermal conductivity via LSM, *Int. J. Heat Mass Transfer*, **126**:1347–1356, 2018, https://doi.org/10.1016/j.ijheatmasstransfer.2018.06.005.
30. M. Usman, Z.H. Khan, M.B. Liu, MHD natural convection and thermal control inside a cavity with obstacles under the radiation effects, *Physica A*, **535**, 2019, https://doi.org/10.1016/j.physa.2019.122443.
31. Y. Zheng, S. Yaghoubi, A. Dezfulizadeh, S. Aghakhani, A. Karimipour, I. Tlili, Free convection/radiation and entropy generation analyses for nanofluid of inclined square enclosure with uniform magnetic field, *J. Therm. Anal. Calorim.*, **141**:635–648, 2020, https://doi.org/10.1007/s10973-020-09497-y.